2004

Air-Side Heat Transfer Augmentation of a Refrigerator Evaporator Using Vortex Generation

Andrew Sommers
University of Illinois at Urbana-Champaign

Anthony M. Jacobi
University of Illinois at Urbana-Champaign

AIR-SIDE HEAT TRANSFER AUGMENTATION OF A REFRIGERATOR EVAPORATOR USING VORTEX GENERATION

A. D. SOMMERS , A. M. JACOBI
Department of Mechanical and Industrial Engineering,
University of Illinois, 1206 W. Green St., Urbana, IL 61801 USA
Phone: (217) 333-4108, Fax: (217) 244-6534, E-mail: a-jacobi@uiuc.edu

ABSTRACT

In air-cooling applications with frost production, heat exchanger performance is often air-side limited, because the two-phase flow of the refrigerant provides excellent heat transfer coefficients, and because designers typically use a large air-side fin spacing for frost tolerance. The large fin spacing prolongs operation of the heat exchanger by mitigating the effect of the accumulating frost, but it does not allow for a very high air-side heat transfer coefficient. Longitudinal vortex generation is a proven and effective technique for thinning the thermal boundary layer and enhancing heat transfer, but its efficacy in a frosting environment is essentially unknown. In this study, an array of delta-wing vortex generators is applied to a plain fin-and-tube heat exchanger with a fin spacing of 8.5 mm. Heat transfer and pressure drop performance are measured to determine the effectiveness of the vortex generator under frosting conditions. For Reynolds numbers between 500 and 1200, a reduction of 35.0% to 42.1% is observed in the air-side thermal resistance. Correspondingly, the heat transfer coefficient is observed to be between 33-53 W/m^2-K for the enhanced heat exchanger and between 18-26 W/m^2-K for the baseline heat exchanger. A modified volume-goodness parameter is also calculated and shows that the enhanced exchanger outperforms the baseline specimen for the range of Reynolds numbers examined.

1. INTRODUCTION

Plain fin-and-tube heat exchangers having a large fin spacing (i.e. 5-10 mm) are used in certain frosting applications because of their reliability, cost-effectiveness, and relative tolerance to frost accumulation. Unfortunately, this heat exchanger geometry is thermally inefficient, and the air-side convective coefficients associated with these units are relatively small in comparison to more highly compact designs. The design limitations imposed upon these heat exchangers require new and innovative approaches to further reduce the core volume, material cost, and flow noise. Because the air-side thermal resistance is dominant in these applications, even modest enhancements in the air-side thermal-hydraulic performance could lead to smaller, lighter, and more energy efficient systems. The purpose of this research is to provide a fundamental understanding of the enhancement capability of vortex generators (VGs) as an air-side enhancement technique for heat exchangers with large fin spacing in frosting applications. Specific objectives of this study include evaluating the performance of delta-wing vortex generators under low airflow rates, their efficacy downstream from the leading edge, and their tolerance to frost accumulation. Frost properties are evaluated by calculating a time-varying interfacial frost surface temperature, and the frost thickness is found by numerically integrating mass deposition rate data measured in the wind tunnel.

Streamwise vortex enhancement works by imparting a secondary flow to the mainstream, which brings a swirling flow in contact with the boundary layer on the surface of the fin. The downwash region of the vortex thins the thermal boundary layer, whereas the upwash region thickens it. These surface-normal inflow and outflow regions occupy nearly the same surface area, but the convective response is nonlinear and a net heat transfer enhancement is manifest. This enhancement comes at the cost of an increased pressure drop due to the form drag on the vortex generators, but this incremental increase in pressure drop is relatively small for a plain fin-and-tube heat exchanger where the major source of drag is the tubes.

Several researchers have demonstrated the clear promise of vortex generation as a heat transfer enhancement method. For instance, Fiebig (1998) concluded that local heat transfer enhancements of 100% and overall enhancements of 50% were possible. He also reported that vortex generators inserted into channel flow might

produce turbulent flow instabilities for Reynolds numbers as low as 350. In a recent study using delta winglets, Kwak *et al*. (2002) observed heat transfer improvements of 10-25% with a corresponding increase in pressure losses of 20-35% in a multi-channel test core using a three-row, circular tube bundle in an in-line arrangement. Full-scale implementation and testing of vortex generators in heat exchangers, however, is only sparsely reported in the literature. In one of two known experiments using rectangular winglets, Russell *et al*. (1982) reported an enhancement of 47% in the *j* factor accompanied by a 30% increase in the *f* friction factor for a Reynolds number of 500 based on hydraulic diameter. In a second, more recent full-scale experiment of delta-wing vortex generators on a plain-fin-and-tube heat exchanger, El Sherbini and Jacobi (2002) showed considerable heat transfer augmentation with little to no associated pressure drop penalty. For the present study, the dimensions and angle of attack of the VG array were selected on the basis of an extensive parametric study performed by Gentry and Jacobi (1997) for a single delta wing in developing channel flows.

Aside from early work by Storey and Jacobi (1999) for a channel flow, we are aware of no research reported in the open literature on the use of vortex generators with simultaneous heat and mass transfer. Because of the breadth of the technical literature on frost, only those findings highly germane to this study are discussed. Östin and Andersson (1991) observed monotonic and cyclic frost growth patterns and found that for times greater than 60 minutes, the mass flux of condensing water vapor contributes nearly equally to increasing frost density as it does frost thickness. Le Gall and Grillot (1997), in deriving a one-dimensional transient model for the prediction of frost growth and densification on a cold surface, observed that the transport of water vapor into the frost layer was often significantly higher than that due to simple Fickian diffusion. Finally, Rite and Crawford (1991) found that while holding the airflow rate constant, the overall thermal conductance increased as frost was deposited on the coil, a phenomenon they attributed to an increased heat transfer coefficient and added surface roughness from the frost.

2. EXPERIMENTAL METHOD

2.1 Air-Side Loop

The experiments were conducted in a closed-loop wind tunnel comprised of 5 major sections: a thermal-conditioning chamber, flow-conditioning chamber, contraction, test section, and return loop as detailed by Davis and co-workers (1996). The temperature and humidity of the air were established inside the thermal-conditioning chamber prior to each experiment using an upstream cooling coil and a controlled steam injection system. The relative humidity in the wind tunnel was preset to 80% before each experimental run, and the air inlet temperature was preconditioned to be between 10 and 11 °C. Accompanying air outlet temperatures ranged from −4 to +2 °C. The core pressure drop of the heat exchanger was measured using four pressure taps (two upstream and two downstream) and a pressure transducer with a span of 250 Pa and an uncertainty of 0.073% full-scale. Air inlet and outlet temperatures were measured using thermopiles placed upstream and downstream of the exchanger. These thermopiles were inserted from both the top and bottom surface of the test section and consisted of five 0.25-mm-diameter, type-T thermocouples calibrated against NIST-traceable ASTM thermometers. The resulting uncertainty in the average air temperature was ±0.1 °C. The velocity of the approach air was measured using thermal anemometry with a maximum uncertainty of approximately ±0.06 m/s. The velocity profiles were shown to be flat within ±4.3% for the lowest test velocity (0.46 m/s) and ±5.7% for the highest test velocity (2.0 m/s).

2.2 Coolant Loop

The refrigerant was a 40% mixture by weight of ethylene glycol (DOWTHERM 4000) and water. The inlet and outlet fluid temperatures were measured using platinum RTDs with an uncertainty of ± 0.017 °C. The coolant inlet temperature was maintained at –12 to –13 °C for each experiment. Mixing cups and 90° elbows were incorporated into the piping network upstream of the RTDs to ensure a well mixed, bulk fluid temperature. A Coriolis-effect flow meter was installed downstream from the heat exchanger to measure the coolant mass flow rate with an uncertainty of ± 0.4%. The baseline heat exchanger specimen used for conducting this comparison was of a plain fin-and-tube construction with a fin spacing of 8.47 mm, where the fins were brazed to the tube in order to eliminate an unknown thermal contact resistance. The dimensions of the heat exchanger were 451 mm x 203 mm x 51 mm, and the hydraulic diameter before frosting was 10.2 mm. Heat transfer data from the exchanger were acquired every 5 minutes following an initial frost growth period of 30 minutes. For the enhanced heat exchanger, vortex generators were attached to the fin surface according to the pattern shown in Figure 1.

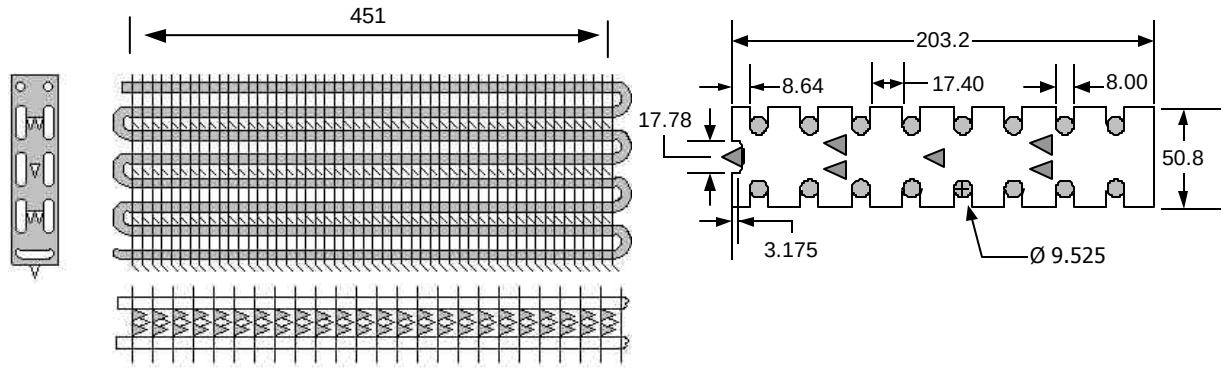

Figure 1: Heat exchanger geometry and vortex generator configuration

2.3 Vortex Generator Geometry

The delta wing vortex generators were cut from standard 0.254 mm aluminum shim stock using wire electrical discharge machining (EDM). They were made with an aspect ratio, Λ, of 2.0 and placed on the heat exchanger with an angle of attack, α, of approximately 55°. They were attached to the fin surface at intervals of 51 mm using double-sided tape. The addition of the vortex generators to the heat exchanger increased the total air-side area by only 3.1%. All relevant wing dimensions are provided below in Figure 2.

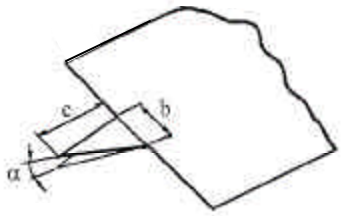

Wing span, b (mm)	10.5
Wing chord, c (mm)	10.5
Chord to hydraulic dia.	1.027
Aspect ratio, Λ=2b/c	2.0
Angle of attack, α	55°

Figure 2: A vortex generator of chord length, c, base length, b, and angle of attack, α

3. DATA INTERPRETATION

Energy balances were monitored to ensure fidelity of all measured data. For 80% of the data points reported, the maximum energy transfer difference was 8.3% while the remaining 20% of the data had energy balances between 8.4-10%. An ε-NTU method was then utilized to interpret the performance of the heat exchanger. For the geometry studied, the exchanger could be divided into two partitions along an adiabat with each partition containing 8 passes in cross-flow. The upper partition (stream 1) had an overall counter flow arrangement while the lower partition (stream 2) had an overall parallel flow arrangement. Total energy balances were written for each partition and each stream, and two ε-NTU equations were used to complete the system of equations following an approach similar to that used by Davis (1996). In the ε-NTU equations, the maximum realizable enthalpy difference was written for the air stream in each partition. Appropriate relations for the counter-flow partition effectiveness e_1 and the parallel flow partition effectiveness e_2 have been given by Shah and Mueller (1985), and these values could be related to the pass effectiveness ε_p for simple cross flow with the heat rate capacity C_{min} mixed and C_{max} unmixed to calculate the number of transfer units per pass, NTU_P. Thus, the thermal conductance per pass, UA_P, could be determined, and the total thermal conductance, UA_{tot}, could be found by summing over all passes.

The total thermal resistance, R_T, which equals $1/UA_{tot}$, can in turn be represented as a series of individual resistances equivalent to the sum of the refrigerant convection resistance ($R_{r\text{-}conv}$), tube wall conduction resistance ($R_{t\text{-}cond}$), frost conduction resistance (R_{frost}), and air-side convection resistance, (R_{as}), where the frost resistance and air-side resistance are each independently comprised of parallel resistances contributed by the tube and fin. The tube-side convection resistance was found using the Gnielenski correlation and the Colebrook correlation because of their suitability for the range of Reynolds numbers in these tests. The frost conduction resistance was approximated using the Hayashi (1977) correlation for frost density,

$$r_f = 650 \exp(0.277 \cdot T_s), \tag{1}$$

the Lee *et al*. (1997) correlation for frost thermal conductivity,

$$k_f = 0.132 + 3.13e^{-4} r_f + 1.6e^{-7} r_f^2, \tag{2}$$

and the following equations:

$$\frac{1}{R_{frost}} = \frac{k_f \cdot A_{fin}}{d_f} + \frac{2pL_{tube}N_{tubes}k_f}{\ln((D_o + 2d_f)/D_o)} \tag{3}$$

$$\dot{m}_{frost} = \dot{m}_{air,up} mf_{w,up} - \dot{m}_{air,down} mf_{w,down} \tag{4}$$

$$d_f = \int_0^t \dot{m}_{frost}/(A_{tot} \cdot r_f) dt \tag{5}$$

where $mf_{w,up}$ and $mf_{w,down}$ represent the mass fractions of the water in the air upstream and downstream respectively, T_s represents the interfacial surface temperature of the frost, and δ_f represents the frost thickness. From this information, the reciprocal of the refrigerant Nusselt number was plotted along the abscissa, and the total thermal resistance R_T at fixed air-side conditions was plotted along the ordinate to form a so-called Wilson plot. A line was then fit to the data by the method of least-squares, and the overall air-side resistance of the heat exchanger was inferred from a Wilson plot by extrapolating to the ordinate intercept. Here the tube-side refrigerant Nusselt number is infinite (i.e. $1/Nu_R = 0$) so the tube-side convection resistance is zero by definition. As a result, the intercept equals the air-side convective resistance plus the conduction resistance contributed by the frost and the tube wall-both known quantities. Because the tube wall conduction resistance is negligible, the frost resistance can be added to the convective resistance to form an overall air-side thermal resistance, which serves as a convenient basis of comparison for these tests.

Frost properties were evaluated using an average frost surface temperature, T_s, inferred using the heat-and-mass transfer analogy by relating the frost mass deposition rate to the log-mean humidity ratio difference between the air and the frost surface. In this way, the humidity ratio, ω_s, (and hence temperature T_s) at the frost surface could be calculated using the following relationship

$$\dot{m}_{frost} = \frac{h}{c_{p,air}} A_{tot} Le^{-2/3} \Delta w_{lm}, \tag{6}$$

where

$$\Delta w_{lm} = \frac{(w_{up} - w_s) - (w_{down} - w_s)}{\ln[(w_{up} - w_s)/(w_{down} - w_s)]} \tag{7}$$

and Le is the Lewis number and A_{tot} is the total heat transfer surface area.

Performance evaluation criteria are often used to assess the merits of heat transfer enhancement techniques. The London area-goodness factor, which is defined as the ratio of the Colburn *j*-factor over the friction factor, *f*, is a commonly used metric because it examines the intrinsic link and tradeoff between heat transfer enhancement and increased frictional forces in air flow over surfaces. Higher *j/f* ratios usually mean better performance, however, the use of *j/f* is restrictive because it does not explicitly account for blower power. For this reason, a modified volume-goodness factor, Θ, was used in this analysis instead. Formally, this PEC is defined as

$$\Theta = \frac{q_{air}}{(V_{core} \cdot \Delta h_{lm})}, \tag{8}$$

where V_{core} is the exchanger core volume, q is the heat transfer rate of the air stream, and Δh_{lm} is the log-mean enthalpy difference. It is common to plot Θ against blower power.

4. RESULTS AND DISCUSSION

The thermal-hydraulic performance of the evaporator was measured before and after the addition of the delta-wing vortex generators. In order to assess the pressure drop penalty associated with the enhanced geometry, the delta wing array was tested over several airflow rates under dry conditions. The results reveal a pressure drop increase associated with the delta wings under dry conditions that varies between 64% for Re_{dh} = 1550 and 275% for Re_{dh} = 830 with an uncertainty in the measurements of 2.4% and 28.8%, respectively. The total core pressure drop (i.e. 1.74 – 4.83 Pa), however, is small compared to overall system losses, and it should be noted that the incremental fan power needed to overcome this deficit would always be less than 0.15 watts when using this enhanced geometry under dry conditions. Under frosted conditions, the pressure penalty ranged from 4.0 to 11.9 Pa with an associated incremental fan power requirement of ≤ 0.33 watts.

For Re_{dh} = 500-1200, a consistent reduction of 35.0% to 42.1% in the overall air-side thermal resistance was observed for the enhanced evaporator as shown in Figure 3. (As discussed in the methodology, the overall air-side resistance is the sum of the conduction resistance due to the frost and the convective resistance due to the air stream and therefore reflects the total effect that vortex generation has on both the growth of the frost layer and the thermal boundary layer at the surface.) The presence of frost on the heat exchanger has been shown to contribute a conduction resistance up to 0.012 K/W.

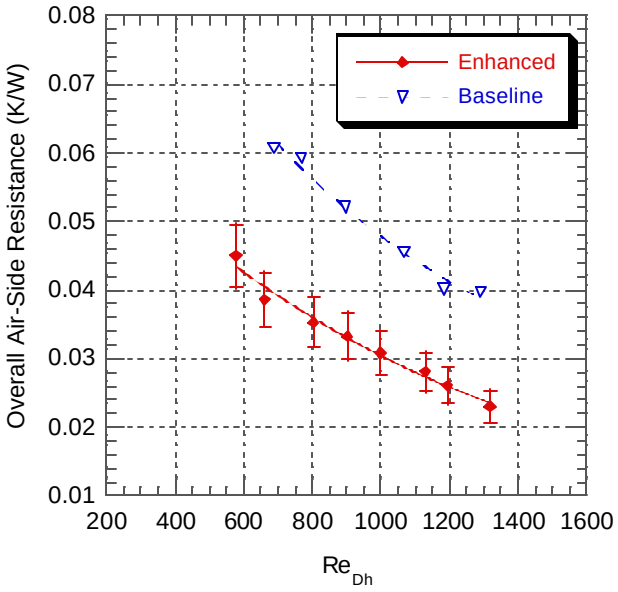

Figure 3: The overall air-side thermal resistance is 35% to 42% lower for the enhanced evaporator.

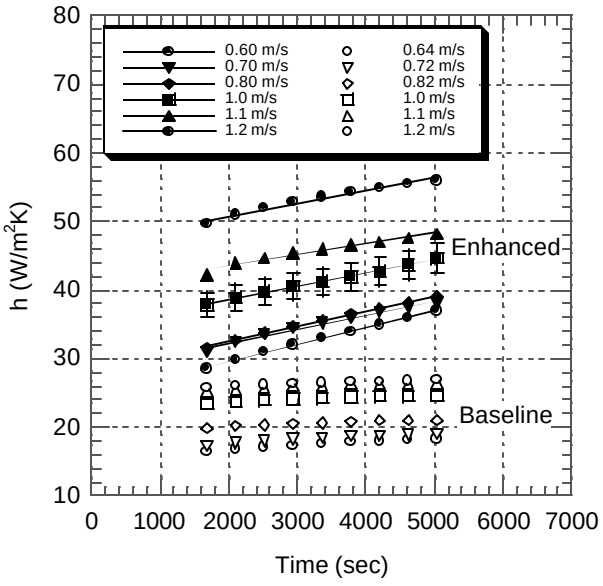

Figure 4: The heat transfer coefficient plotted as a function of face velocity and deposition time.

This reduction in air-side resistance can be largely ascribed to increased convection and flow mixing in the finned channels and is reflected in the behavior of the convective heat transfer coefficient, which was observed to increase by 60% to 93% over the range of tested air velocities as shown in Figure 4. Because non-conducting tape was used to attach the delta wings and the wing-to-total area ratio was 3.1%, these enhancements could be entirely attributed to the streamwise vortices. The value of the heat transfer coefficient varied from 33-53 W/m^{2}K for the enhanced configuration and from 18-26 W/m^{2}K for the baseline configuration.

The observed increase in the air-side heat transfer coefficient with respect to time as shown in Figure 4 is best attributed to the growing frost layer and a few different mechanisms associated with it. First, the frost provides an added roughness to the surface area of the evaporator, which may serve to "trip" the boundary layer from laminar to turbulent flow more quickly than a smooth surface. The consequence of turbulent flow is higher Nusselt numbers and delayed boundary layer separation from the cylindrical surface of the tube. As the frost develops in time and

becomes increasingly more dendritic, the location of boundary layer transition gradually begins to shift toward the front of the coil and more of the evaporator experiences a turbulent flow regime. As this happens, the average convective coefficient begins to increase. The second mechanism responsible for this overall increase in the heat transfer coefficient is the narrowing of the air passages due to frost buildup while constant total air mass flow rate is maintained through the coil. The result is an increase in the local air velocity and a reflected increase in the convective coefficient. Third, because the growing frost layer is composed of dendritic spires, the frost may behave as an additional extended surface for heat transfer. In this way, the frost increases the heat transfer surface area of the coil and can produce a small increase in the convective coefficient.

In Figure 5, the modified volume-goodness factor is plotted versus blower power. Several trends can be identified. First, the volume-goodness factor increased with increasing Reynolds number, an observation consistent with expectation. This simple fact confirms that heat transfer is augmented at higher air flow rates. Second, it is important to note that the performance decreased in time as frost accumulated on the evaporator emphasizing the frost layer as an additional thermal resistance. Third, this deterioration in performance with time was more pronounced at lower Reynolds numbers. This fact suggests that the properties of the growing frost layer are different at lower Reynolds numbers than at higher Reynolds numbers and corroborates other data, which suggest that the frost is more dendritic at lower air flow rates. Dendritic frost, of course, poses a greater conduction resistance than dense frost. It is also readily apparent from this comparison that the VG array appears to be beneficial over the entire range of Reynolds numbers examined. The net enhancement in the volume-goodness factor was 16.7% to 32.9% over the range of face velocities tested. The maximum uncertainty in the modified volume-goodness factor was approximately 1.8%

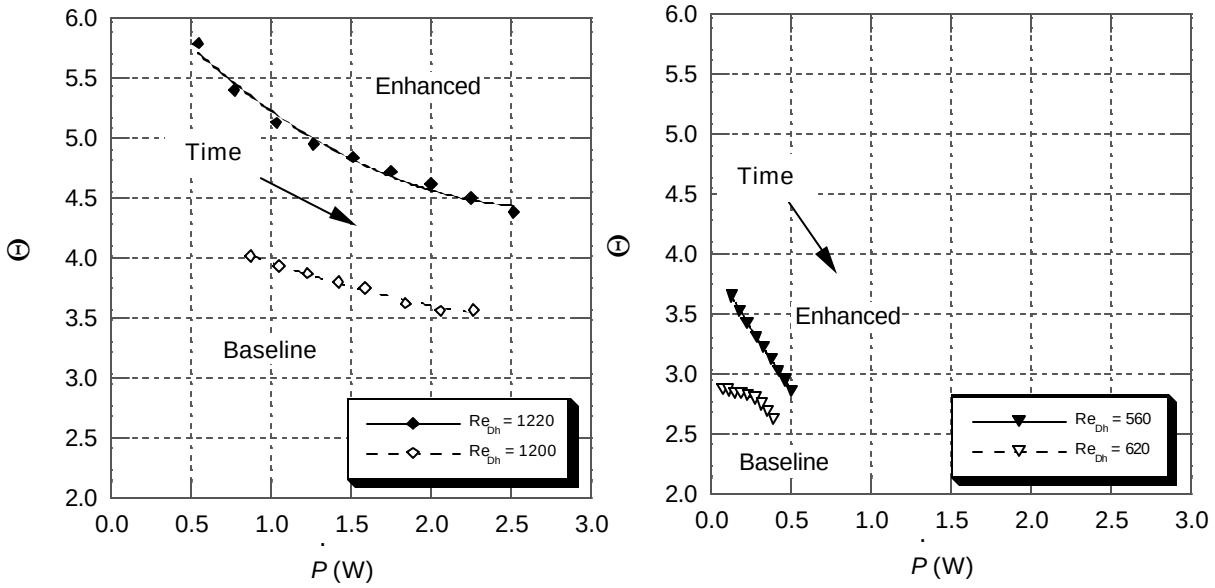

Figure 5: The modified volume-goodness factor reveals an enhancement of 17% to 33%.

The effect of vortex generation on frost properties was also qualitatively examined. As shown in Figure 6, the average density of the frost layer accumulating on the enhanced evaporator was approximately 31 kg/m^3 greater than the average density on the baseline evaporator, which amounts to a 26% increase in frost density. This phenomenon, already observed in channel flow by Storey and Jacobi [6], is probably due to the flow behavior in the downwash region behind the delta wing where the vortex suppresses the axial growth of frost spires and promotes dendritic branching. Because the frost is denser on the enhanced evaporator, the conduction resistance through the frost layer is reduced permitting the convection of more heat away by bulk flow. This observation was also reflected in the numerically calculated frost thicknesses. The numerically integrated frost thickness on the baseline evaporator was on average 0.4-0.8mm thicker than the frost layer on the enhanced evaporator.

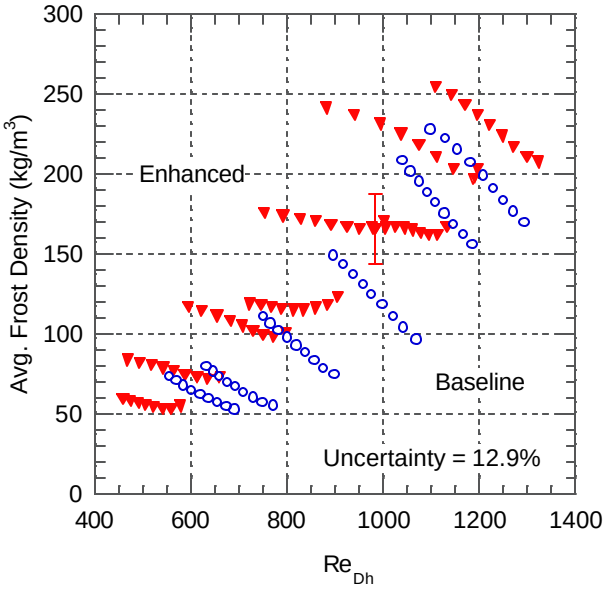

Figure 6: Frost density calculated from mass deposition rate data

5. CONCLUSIONS

In this study, a full-scale heat exchanger was tested before and after the addition of several delta wing vortex generators. The tested heat exchanger was a brazed fin-and-tube evaporator with a fin spacing of 8.47 mm and is currently in production for use in domestic refrigeration. The examined vortex generator array was a 4-row, staggered configuration where the delta wings were attached in an alternating single row, double row arrangement at a core depth interval of 50.8 mm (2 in). For Reynolds numbers between 500 and 1200, which corresponds to face velocities between 0.52 m/s and 1.2 m/s, the air-side thermal resistance was shown to decrease by 35% to 42% with the addition of the delta wings while the convection heat transfer coefficient increased by 60% to 93%. Typical values for the heat transfer coefficient for the enhanced case were 33-53 W/m^2-K, and typical values for the baseline case were 18-26 W/m^2-K. A modified volume-goodness factor was also calculated and suggested that the delta-wing-enhanced heat exchanger was superior to the baseline heat exchanger over the entire range of Reynolds numbers tested. An average frost density was calculated from mass deposition rate data and revealed that the frost densities were greatest for the enhanced data, suggesting that vortex-induced flow suppresses dendritic frost growth. This conclusion is further supported by the frost thickness data and is an important discovery because it suggests that frost grown under enhanced conditions may possess a higher thermal conductivity and therefore may pose a smaller conduction resistance.

NOMENCLATURE

A_{tot}	total heat transfer surface area	(m^2)	**Greek Symbols:**	
A_{min}	minimum free flow area	(m^2)	δ	frost thickness
C	heat-rate capacity, $\dot{m} c_p$	(W/K)	ε	effectiveness, q/q_{max}
D_h	hydraulic diameter, $D_h = 4A_{min}L/A_{tot}$	(m)	ν	kinematic viscosity
D_o	outside tube diameter	(m)	Θ	volume-goodness factor
h	heat transfer coefficient	(W/m^2·K)	Λ	delta-wing aspect ratio
k	thermal conductivity	(W/m·K))	ρ	density
L	fin length	(m)	ω	humidity ratio
L_{tube}	tube length per pass	(m)		

Le	Lewis number	(−)	**Subscripts:**	
$\dot{m}$	mass flow rate	(kg/s)	as	air-side
$\dot{m}_f$	frost deposition rate	(kg/s)	ai	air at the exchanger inlet
mf	water vapor mass fraction	(−)	f	frost
N	number of tubes, fins, etc.	(−)	lm	log-mean difference
$\dot{P}$	pumping power	(W)	max	maximum
ΔP_{core}	air-side core pressure drop	(Pa)	min	minimum
q	rate of heat transfer	(W)	ri, ro	inlet and outlet refrigerant
R	thermal resistance	(K/W)	rm	refrigerant between partitions
Re_{Dh}	air-side Reynolds number, $V_{max}D_h/\nu$	(−)	s	at the frost surface
t	time	(sec)	t	tube wall
T	temperature	(K)	w	water
UA_{tot}	overall thermal conductance	(W/K)		
V_{max}	maximum air-side velocity	(m/s)		
V_{core}	heat exchanger core volume	(m^3)		

REFERENCES

Davis, M.A., Jacobi, A.M., and Hrnjak, P.S., 1996, "Evaporator Calorimeter: The Study of Overall Heat Transfer Performance," Air Conditioning and Refrigeration Center, ACRC Report TR-107.

El Sherbini, A.I., and Jacobi, A.M., 2002, "The Thermal-Hydraulic Impact of Delta-Wing Vortex Generators on the Performance of a Plain-Fin-and-Tube Heat Exchanger," *Int. J. HVAC&R Research*, vol. 8, no. 4: p. 357-370.

Fiebig, M., 1998, "Vortices, Generators, and Heat Transfer," *Trans. IChemE*, vol. 76, no. A: p.108-123.

Gentry, M.C. and Jacobi, A.M., 1997, "Heat Transfer Enhancement by Delta-Wing Vortex Generators on a Flat Plate: Vortex Interactions with the Boundary Layer," *Exp. Therm. Fluid Sci*., vol. 14: p. 231-242.

Hayashi, Y., Auki, A., Adachi, S., and Hori, K., 1977, "Study of Frost Properties Correlating with Frost Formation Types," *J. Heat Transfer*, vol. 99: p. 239-245.

Kwak, K.M., Torii, K., and Nishino, K., 2002, "Heat Transfer and Flow Characteristics of Fin-Tube Bundles with and without Winglet-Type Vortex Generators," *Experiments In Fluids*, vol. 33: p. 696-702.

Lee, K.S., Kim, W.S., and Lee, T.H., 1997, "A One-Dimensional Model for Frost Formation on a Cold Flat Surface," *Int. J. Heat Mass Transfer*, vol. 40, no. 18: p.4359-4365.

Le Gall, R. and Grillot, J.M., 1997, "Modeling of Frost Growth and Densification," *Int. J. Heat Mass Transfer*, vol. 40, no. 13: p. 3177-3187.

Östin, R. and Andersson, S., 1991, "Frost Growth Parameters in a Forced Air Stream," *Int. J. Heat Mass Transfer*, vol. 34, no. 5: p. 1009-1017.

Rite, R.W. and Crawford, R.R., 1991, "The Effect of Frost Accumulation on the Performance of Domestic Refrigerator-Freezer Finned-Tube Evaporator Coils," *ASHRAE Transactions*, vol. 97, no. 2: p.428-437.

Russell, C.M.B, Jones, T.V., and Lee, G.H., 1982, "Heat Transfer Enhancement Using Vortex Generators," *Proc. 7th Heat Transfer Conference*, vol. 3: p. 283-288.

Shah, R.K., Mueller, A.C., 1985, "Heat Exchangers," *In:* Rohsenow W.M., Hartnett, J.P., and Gani′c, E.N., eds., *Handbook of Heat Transfer Applications*, McGraw-Hill, New York: p. 4.11-15.

Storey, B.D. and Jacobi, A.M., 1999, "The Effect of Streamwise Vortices on the Frost Growth Rate in Developing Laminar Channel Flows," *Int. J. Heat Mass Transfer*, vol. 42: p. 3787-3802.